Analytica Chimica Acta 1181 (2021) 338863

Contents lists available at ScienceDirect

Analytica Chimica Acta

journal homepage: www.elsevier.com/locate/aca

Electrochemical detection of hepcidin based on spiegelmer and MoS_2NF-GNR@AuNPs as sensing platform

Shilpa Rana [a], Amandeep Kaur [a], Anu Bharti [a], Suman Singh [b], Archana Bhatnagar [a], Nirmal Prabhakar [a, *]

[a] Department of Biochemistry, Sector-25, Panjab University, Chandigarh, 160014, India
[b] CSIR- Central Scientific Instruments Organization, Sector-30-C, Chandigarh, 160030, India

HIGHLIGHTS

- Spiegelmers are mirror-image L-RNA oligonucleotides possessing higher resistance to degradation by nucleases.
- An electrochemical spiegelmer sensor was constructed based on MoS_2NF-GNR@AuNPs.
- EIS response was measured for detection of hepcidin.
- The sensing platform displayed wide linear range and low detection limit.
- The spiegelmer sensor was applied to detect hepcidin in spiked-in human serum sample.

GRAPHICAL ABSTRACT

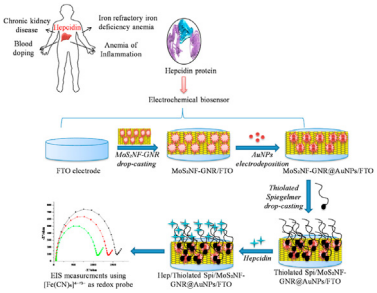

ARTICLE INFO

Article history:
Received 22 May 2021
Received in revised form
2 July 2021
Accepted 19 July 2021
Available online 26 July 2021

Keywords:
Graphene nanoribbon
Molybdenum disulfide nanoflowers
Spiegelmers
Electrochemical impedance spectroscopy

ABSTRACT

Spiegelmers, mirror image L- RNA oligonucleotides, possesses high plasma stability and non-immunogenicity. Herein, a novel spiegelmer based impedimetric biosensor grafted with Au nanoparticles and molybdenum disulfide nanoflowers/graphene nanoribbons nanocomposite has been designed to detect hepcidin in spiked-in human serum sample. Firstly, molybdenum disulfide nanoflowers/graphene nanoribbons (MoS_2NF-GNR) hybrid was drop-casted onto the FTO electrode followed by electro deposition of Au nanoparticles (AuNPs). Hepcidin specific thiolated spiegelmer was then immobilized on the MoS_2NF-GNR@AuNPs for hepcidin detection. Electrochemical impedance spectroscopy was used to assess the performance of the sensing platform based on the variation of charge transfer resistance (ΔR_{ct}) relative to the $Fe(CN)_6^{4-/3-}$ electrochemical probe in the presence of hepcidin. The impedance signals were recorded at the frequency range of 10^{-1} to 10^5 Hz and potential was set as 0.18 V. Under optimized conditions, the limit of detection of spiegelmer based sensor for hepcidin was 0.173 $pgmL^{-1}$ within a wide linear range of 0.005–10 $ngmL^{-1}$. The biosensor possesses selectivity, acceptable reproducibility with RSD as 4.76% and stability for up to 20 days. The satisfactory recovery result (89.8–103.1 %) in human serum indicates that the sensor has applicability in clinical monitoring of hepcidin.

* Corresponding author.
E-mail addresses: nirmalprabhakar@pu.ac.in, nirmalprabhakar@gmail.com (N. Prabhakar).

https://doi.org/10.1016/j.aca.2021.338863
0003-2670/

1. Introduction

Ultrasensitive detection of hepcidin, a liver synthesized peptide hormone, is extremely essential for early diagnosis of iron-related disorders as well as for examining erythropoietin blood doping [1]. Though there are conventional methods for the detection of hepcidin such as mass spectrometry [2,3] and ELISAs [4], but they are time-consuming and require trained personnel for handling the expensive instruments or the reagents. To overcome these limitations, the SPR-based biosensors have been developed for hepcidin detection, however, they lack the real sample analysis for clinical applicability [5,6]. In addition, the SPR-based biosensors are less sensitive towards low molecular weight molecules due to the minute and nonspecific changes in the refractive index. Infact, the electrochemical biosensors are more advantageous than SPR-based biosensors in terms of affinity and sensitivity. For instance, gold-silver core shell nanoparticles based electrochemical immunosensor could detect hepcidin as low as 0.857 pgmL^{-1}, which is so far the lowest limit of detection amongst the other reported biosensors or traditional methods. However, the biorecognition molecule i.e. antibodies are expensive to produce and have poor stability as compared to RNA oligonucleotides. The aptamers have better sensitivity than antibodies, thus, benefits in achieving lower detection limit.

Spiegelmers are synthetic oligonucleotides with L-configuration which not only show high affinity and selectivity towards the ligand but also possesses biostability due to the resistance against enzymatic degradation in biological fluids [7]. A study by Schwoebel et al. [8] reported that hepcidin spiegelmer binds to hepcidin with high affinity showing dissociation constant of 0.65 ± 0.06 nmol L^{-1}. Since the biological fluids comprises of various nucleases which are stereospecific, spiegelmers have an advantage over conventional aptamers as these are L-nucleotides that do not occur naturally and therefore resistant to nucleases. In addition, the modification of conventional aptamers is cumbersome due to the exchange of unprotected nucleotides while maintaining the overall conformation [9]. The synthesis of spiegelmers involves the chiral form of target and D-form oligonucleotides during SELEX process followed by chemical synthesis to prepare L-form target. These macromolecules require fewer resources for production and are inexpensive as compared to other mimicking molecules [10].

The sensing platform of the biosensor has a crucial role in improving the sensitivity and thus nanomaterials are widely used for their fabrication. The carbon-based nanomaterials such as fullerenes, carbon nanotubes (CNTs), carbon-black, graphene and its derivatives have become increasingly popular as a nanocomposite for electrode fabrication. Due to the large surface area, greater electroconductivity and excellent stability, CNTs are suitable for electrochemical sensing [11,12]. Recently, Paulo et al. [13] developed a wearable glove-based biosensor embedded with carbon spherical shells and printex carbon nanoballs for the detection of carbendazim, diuron, and paraquat and fenitrothion with LOD as 4.7 × 10^{-8} mol L^{-1}, 9.2 × 10^{-7} mol L^{-1}, 2.4 × 10^{-8} mol L^{-1} and 6.4 × 10^{-7} mol L^{-1}, respectively. Another study by Anderson et al. [14] reported the electrochemical detection of paracetamol in sweat, saliva and urine with detection limit of 120, 286 and 584 nmol L^{-1}, respectively. Graphene nanoribbons (GNRs), on the other hand, have greater electron transfer rate due to easier ion diffusion through thinner ribbons and have high aspect ratio than pure graphene and hence considered to be a potential fabrication nanomaterial [15,16]. Besides, due to the structural resemblance to graphene, molybdenum disulfide (MoS_2)- a transition metal dichalcogenides-has received interest in biosensors applications [17]. Moreover, the MoS_2 nanostructures embedded on GNRs acts a support for the faster permeation of electrolytes [18]. Hence, the combined properties of MoS_2-GNR hybrid provides better electrochemical performance by accelerating electron transfer [19,20]. Zhao et al. [21] constructed a sensor to detect quercetin based on MoS_2-GNR hybrid nanocomposite and exhibited good performance with detection limit of 0.82 nM. Facure et al. [22] designed an impedimetric biosensor containing graphene oxide and MoS_2 to detect antibiotics in liquid media and achieved LOD as 0.5 nM.

In the MoS_2-GNR hybrid sensing matrice, MoS_2 is used as a supporting material as the unbound sulfur groups on the stacked S−Mo−S held together by van der Waal interactions acts as a binding group for metal nanoparticles [23]. These MoS_2 nanosheets provide a greater surface area for deposition of metallic nanoparticles, thereby, enhancing the electrocatalytic properties due to synergistic effect [24,25]. Metallic nanoparticles have gained enormous attention due to high electrocatalytic activities, better sensitivity and excellent biocompatibility which helps in holding the biorecognition receptors such as antibodies or aptamers while conserving their functionality. Gao et al. [26] developed Au@Pd/MoS_2@MWCNTs based electrochemical immunosensor for detecting hepatitis B e antigen with limit of detection as 26 fgmL^{-1}.

Herein, we demonstrate a first spiegelmer anchored impedimetric biosensor for the detection of hepcidin using MoS_2NF-GNR@AuNPs based biosensing platform. The biosensor has been constructed by sequential drop casting MoS_2NF-GNR nanocomposite and electrodepositing Au nanoparticles (AuNPs) by chronoampermetry on the FTO electrode followed by immobilization of thiolated spiegelmer as biorecognition receptor. The electrochemical impedance spectroscopy (EIS) was used to operate the sensor with ferricyanide/ferrocyanide as redox probe. In the presence of hepcidin, the spiegelmer macromolecules capture the ligand, thus, causing the change in impedance signal. The spiegelmer sensor was capable of detecting hepcidin in the picomolar range and exhibited acceptable reproducibility, regeneration and reusability with good shelf-life. The satisfactory analytical performance of the spiegelmer sensor was observed in spiked-in human serum samples promising reliable hepcidin detection for broader applications.

2. Experimental section

2.1. Chemicals and reagents

Human hepcidin-25 trifluoroacetate salt, thiolated spiegelmer, tetrachloroauric acid ($HAuCl_4$), sodium molybdate hydrate ($Na_2MoO_4.H_2O$), thiourea ($SC(NH_2)_2$), somatostatin 28, multi-walled carbon nanotubes (MWCNTs), dimethylformamide (DMF), bovine serum albumin (BSA), fluorine-doped tin oxide (FTO) sheets and human serum were purchased from Sigma-Aldrich Co., Ltd. (St. Louis, MO, USA). Potassium ferrocyanide ($K_4[Fe(CN)_6]$), potassium ferricyanide ($K_3[Fe(CN)_6]$), sodium sulphate and potassium chloride were bought from HiMedia Laboratory Pvt., Ltd. (Mumbai, India). The di-sodium hydrogen phosphate (Na_2HPO_4), sodium dihydrogen phosphate dihydrate ($NaH_2PO_4 \cdot 2H_2O$) were obtained from Thermo Fischer Scientific Pvt. Ltd. (Maharashtra, India). All other chemicals were of analytical grade. The thiolated spiegelmer stock solution (100 μM) was prepared in TE buffer (containing 10 mM Tris HCl; pH-7.5 and 1 mM EDTA; pH-8.0). The stock solution of thiolated spiegelmer was further diluted (10 μM) in freshly prepared TE buffer when used for bioelectrode preparation. The standard hepcidin solution was prepared in 0.1 M phosphate buffer (containing 0.1 M NaH_2PO_4 and 0.1 M Na_2HPO_4; pH-7.0). For preparing spiked-in samples, different concentrations of hepcidin (range- 0.005-10 ngmL^{-1}) were diluted in 10 % human serum at 4 °C.

Hepcidin specific thiolated Spiegelmer sequence [8]: 5'[ThiC6] GCGCCGUAUGGGAUUAAGUAAAUGAGGAGUUGGAGGAAGGGCGC-3′

2.2. Synthesis of MoS_2NF-GNR@AuNPs nanocomposite

The GNRs were prepared by unzipping the MWCNTs as reported in the literature [27]. Briefly, 100 mg MWCNTs were mixed in 50 mL concentrated sulfuric acid and ultrasonified for 2 h. Then, 7 mL phosphoric acid was added and stirred vigorously for about 30 min followed by addition of 2 mM of $KMnO_4$. The suspension was kept at 65 °C for 2 h and then left to cool down. Further, 30 % wt H_2O_2 dissolved in 300 mL of ice water was poured slowly into the above solution. The prepared GNRs were then filtered and collected for further use.

MoS_2NFs were prepared by green hydrothermal method as previously reported in literature [28]. 0.43 g sodium molybdate hydrate and 0.69 g thiourea were dissolved in 80 mL of ultrapure water followed by addition of 0.46 g citric acid with continuous stirring for about 20 min. Next, the homogeneous solution was heated at 190 °C for 24 h in a Teflon-lined stainless steel reactor (autoclave) and the black precipitates obtained were dried (70 °C for 12 h) and collected for further use.

For the preparation of MoS_2-GNR hybrid, 100 μL MoS_2NFs (1 $mgmL^{-1}$; dissolved in DMF) and 200 μL GNRs (1 $mgmL^{-1}$; dissolved in DMF) were mixed and then ultrasonificated for 2 h at power rate of 27 % at 30 °C to form uniform dispersion. Finally, the resultant suspension was filtered and redispersed in DMF for fabrication of the electrode.

2.3. Gold-nanoparticles preparation

The preparation of AuNPs was done by the previously reported Turkevich citrate method [29]. Briefly, 2.5 mM $HAuCl_4$ (10 mL) was added in 1 mM copper (II) sulphate solution (1 mL) and the volume was then made up to 100 mL using ultrapure water. The mixture was stirred and heated to about 90 °C followed by slow addition of 1 % trisodium citrate (5 mL). The color changes from blue to wine red at the end of the reaction indicating successful synthesis of AuNPs.

2.4. Fabrication of MoS_2NF-GNR@AuNPs on the electrode

The schematic illustration of the electrode modification has been depicted in Scheme 1. To construct the proposed spiegelmer sensor, the FTO electrode was washed with 1% acetic acid solution for 30 min and ethanol-water for 5 min under sonification followed by drying. Then, 6 μL of MoS_2NF-GNR suspension was drop casted on the electrode and allowed to dry at room temperature. Finally, the electro deposition of 2.5 mM AuNPs was performed at −0.2 V for 200 s using chronoamperometry.

2.5. Immobilization of Spiegelmer on MoS_2NF-GNR@AuNPs

To immobilize the thiolated spiegelmer, 10 μL of spiegelmer (10 μM) was drop casted one time onto the MoS_2NF-GNR@AuNPs/FTO electrode and allowed to dry at room temperature followed by washing with phosphate buffer (0.1 M; pH-7.4) to remove unbound aptamer from the surface. The fabricated electrodes were stored at 4 °C prior to use. The thiolated spiegelmer shows strong adsorption onto the gold metal surfaces, thus, making stable bioelectrode for capturing the target molecule [30].

2.6. Hepcidin detection

For each electrochemical measurement, different hepcidin concentrations (10 μL) in the range 0.005−10 $ngmL^{-1}$ were incubated for 40 min on the Spi/MoS_2NF-GNR@AuNPs electrode. The relative change in impedance was recorded to calculate the LOD after washing the electrode thoroughly with 0.1 M phosphate buffer (pH 7.0).

All the experiments were performed at room temperature. The electrolyte solution containing 5.0 mM K_3 $[Fe(CN)_6]/K_4[Fe(CN)_6]$ and 0.1 M KCl was used throughout the experiment. The EIS was recorded with the frequency ranging from 10^{-1} to 10^5 Hz at the potential of 0.18 V. The CVs were obtained at potential range of −0.4 V to 1.6 V with a scan rate of 10 mV s^{-1}.

3. Results and discussion

3.1. Principle of electrochemical spiegelmer sensor for hepcidin detection

The spiegelmer sequence is a good candidate for developing an electrochemical biosensor to detect hepcidin due to its high affinity and stability than other biological entities. The spiegelmer binds hepcidin with high affinity ($K_d = 0.65 \pm 0.06$ nmol L^{-1}). Since these are resistant to nucleases degradation, hence, when exposed to biological samples they can detect hepcidin at lower concentration. These advantages allow the biosensor to achieve lowest detection limit towards hepcidin. As illustrated in Scheme 1, the FTO electrode was fabricated with MoS_2NF-GNR@AuNPs nanocomposite which provides high conductivity, excellent biocompatibility and greater surface area for immobilization of thiolated spiegelmer. The Au-thiol linkage allows the stable fabrication of the sensing platform. The redox probe (ferricyanide/ferrocyanide) molecule allows the electron transfer towards the modified electrode with a certain resistance in the absence of hepcidin. In the presence of hepcidin, the spiegelmer folds around the hepcidin and forms a stable complex resulting in resistance escalation as shown in Fig. 2B.

3.2. Morphology of graphene nanoribbons and molybdenum disulfide nanoflowers

The morphologies of prepared GNRs and MoS_2NF were observed through FE-SEM and TEM. As shown in Fig. 1A, the TEM image represents the GNRs formed by unzipping of MWCNTs as ribbon-like structures with a diameter of ~50 nm. The TEM (Fig. 1B) and FE-SEM (Fig. 1D) images of MoS_2NF exhibits flower like structure (average size of 50 nm) with highly dispersed uniformity. The TEM image of MoS_2NF-GNR hybrid (Fig. 1C) shows that the GNRs provides the space for the MoS_2 nanostructures deposition as the inner wall boundaries of CNTs could be slightly seen in the image. The results demonstrate that the nanomaterials were appropriately synthesized for its further use in electrode fabrication.

3.3. Electrode surface analysis

The successful modification of the electrode can be assessed by the change in redox peak in 5 mM ferri/ferrocyanide containing 0.1 M KCl. As seen in Fig. 2A, the conductive nature of MoS_2NF-GNR/FTO (curve b) and MoS_2NF-GNR@AuNPs/FTO (curve c) exhibits an increase in redox peak in comparison to the bare FTO (curve a). However, on spiegelmer immobilization, the peak current decreased (curve d) due to the non-conductive properties of oligonucleotides which hinders the electron transfer. Similarly, after the attachment of hepcidin to the spiegelmer, the redox peak further decreased (curve e) due to target-spiegelmer complex

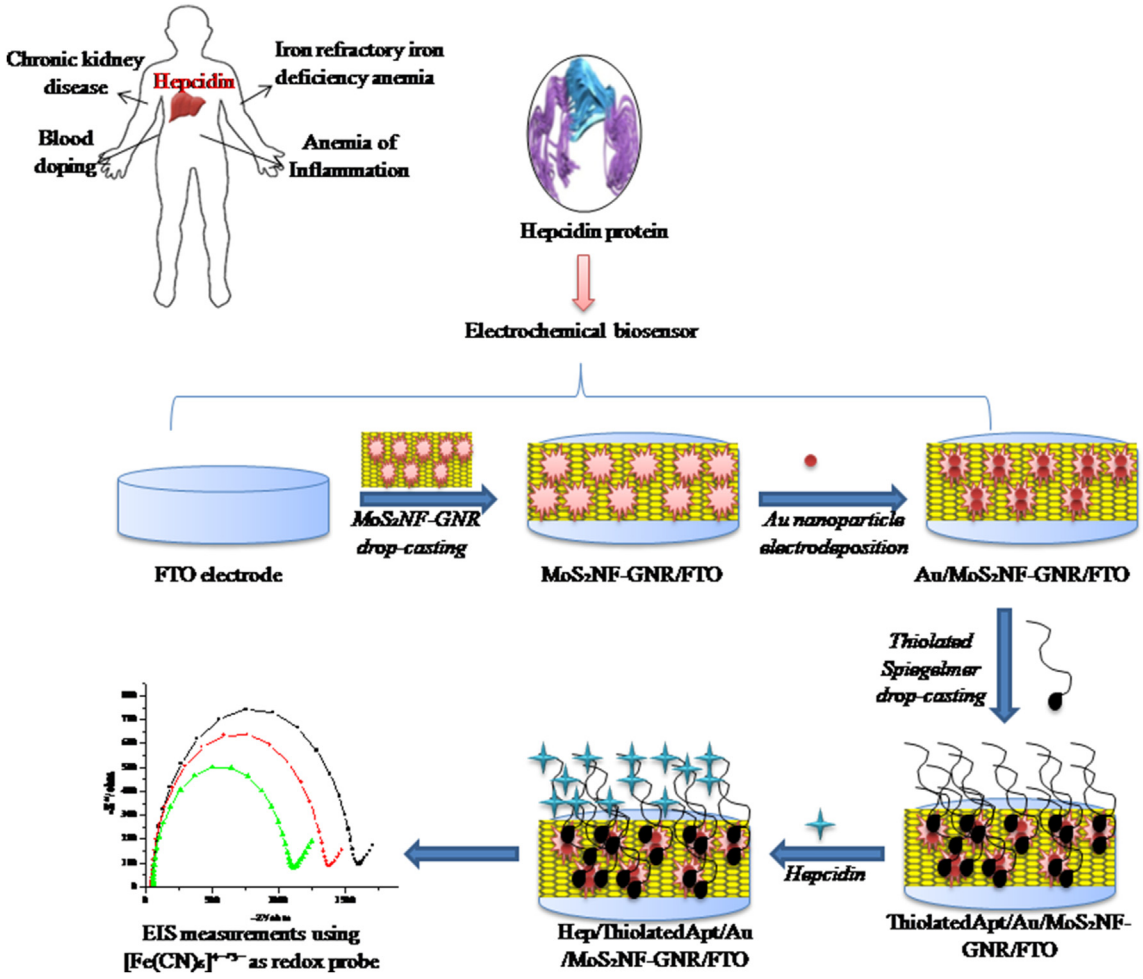

Scheme 1. Schematic illustration of the fabrication steps for constructing spiegelmer sensor to detect hepcidin.

formation which insulated the electrode surface, thus, hindering the electron flow. The peak current of MoS_2NF-GNR@AuNPs/FTO was almost the same for successive cyclic sweeps (Fig. 2A, inset a) indicating the acceptable stability of the modified electrode. To further validate the modification at each step, EIS response was also studied to observe the charge-transfer resistance (R_{ct}). The deposition of MoS_2NF-GNR on the electrode surface resulted in decrease in the R_{ct} value (curve b, R_{ct} = 1.00 kΩ) in comparison to the bare electrode (curve a, R_{ct} = 1.16 kΩ), implying the formation of hybrid nanomaterial layer on the electrode surface. Further, on electrodeposition of AuNPs, a significant decrease in resistance (curve c, R_{ct} = 799 Ω) was observed suggesting the enhanced flow of electron from MoS_2NF-GNR hybrid to AuNPs imposing less resistance for electron transfer towards the redox probe [31]. However, on spiegelmer immobilization on the MoS_2NF-GNR@AuNPs/FTO modified electrode, the R_{ct} increased greatly (curve d, R_{ct} = 1.37 kΩ) confirming the successful anchoring of the spiegelmer on the surface. The incubation of hepcidin on the Spi/MoS_2NF-GNR@AuNPs/FTO biosensor lead to the further increase in the R_{ct} (curve e, R_{ct} = 1.56 kΩ) due to hindrance in the electron mobility on spiegelmer-hepcidin complex formation. The other EIS data like double layer capacity (C_{dl}), admittance to Warburg (Y_o-W) and solution resistance (R_s) have been given in the Supplementary information (Table S2). The CV and EIS results were in line with each other indicating that the modifications on the electrode were successfully carried out.

The XRD spectra of MoS_2NF-GNR@AuNPs and MoS_2NF-GNR are exhibited in Fig. 2C. For MoS_2NF-GNR (Fig. 2C, spectra a), the diffraction peaks at 2θ of 13°, 30° 37.8° and 57.2° can be indexed to 002, 100,103 and 110 MoS_2 crystal planes respectively. The weak peak 2θ of 24.8° represents the 002 diffraction plane of GNR [32]. These characteristics diffraction peaks confirm the formation of MoS_2NF-GNR hybrid. Whereas diffraction peaks of Au in MoS_2NF-GNR@AuNPs (Fig. 2C, spectra b) were observed at 2θ of 36.7° and 40.2° corresponding to 111 and 200 diffraction plane of Au [33].

As shown in Fig. 2D, the IR spectrum of MoS_2NF-GNR/FTO (spectra a) shows the peak at 3387 cm^{-1} (N–H), 1714 cm^{-1} (C=O) and 1571 cm^{-1} (C=C) indicating that MWCNTs oxidized to GNRs and peaks at 482 cm^{-1} (S–S) and 950 cm^{-1} (S–S) depicts the presence of MoS_2NF on the GNRs. Further, the electrodeposition of AuNPs on MoS_2NF-GNR/FTO resulted in the disappearance of the carboxyl-carbonyl (C=O) and aromatic ring (C=C) peaks, and the intensity of the bands at 2800-2950 cm^{-1} range (C–H ring stretching) increases due to the longer alkyl chain (spectra b). In the spiegelmer coated MoS_2NF-GNR@AuNPs (spectra c), the peaks at 1020 cm^{-1} and 1152 cm^{-1} corresponds to the P–O stretch of phosphate backbone of DNA and the other peaks at 1600 cm^{-1} and

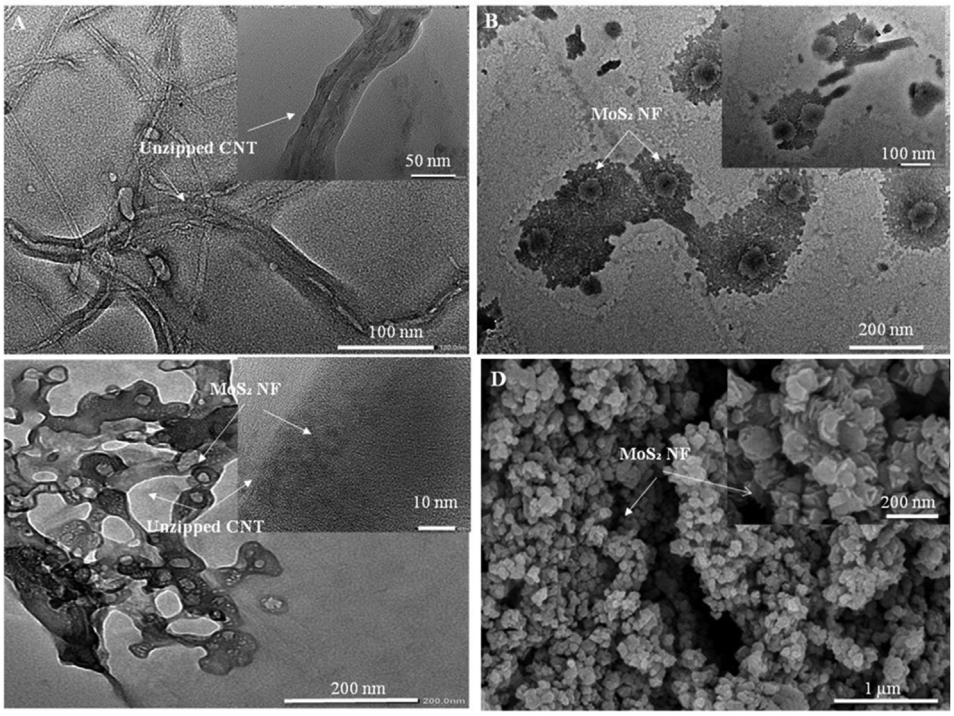

Fig. 1. TEM images of (A) Unzipped MWCNTs, (B) MoS_2NF, (C) MoS_2NF-GNR hybrid; and (D) FE-SEM image of MoS_2NF.

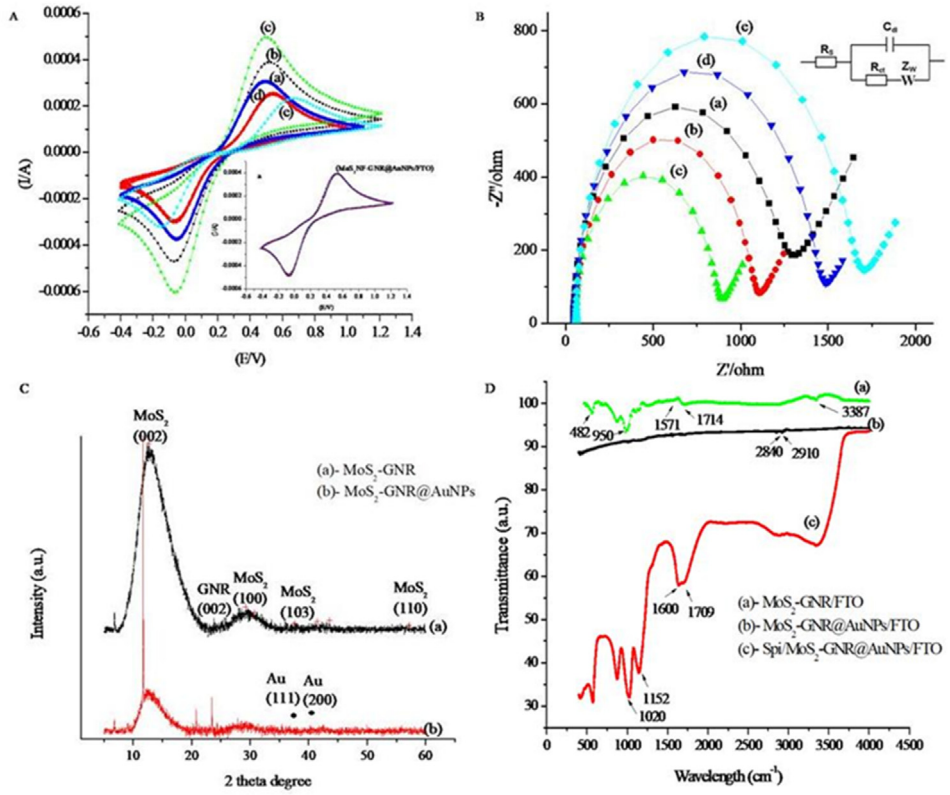

Fig. 2. (A) CV (scan rate of 10 mV s^{-1}); (B) EIS (frequency range of 10^{-1} to 10^5 Hz and potential as 0.18 V) of (a) bare electrode, (b) MoS_2NF-GNR/FTO, (c) MoS_2NF-GNR@AuNPs/FTO, (d) Spi/MoS_2NF-GNR@AuNPs/FTO and (e) Hep/Spi/MoS_2NF-GNR@AuNPs/FTO carried out in electrolyte solution containing 5 mM $[Fe(CN)_6]^{3-/4-}$ and 0.1 M KCl; inset depicts the fitted equivalent circuit in the presence of the redox probe; (C) X-ray diffraction data of nanomaterials; and (D) FTIR spectra of various modified electrodes.

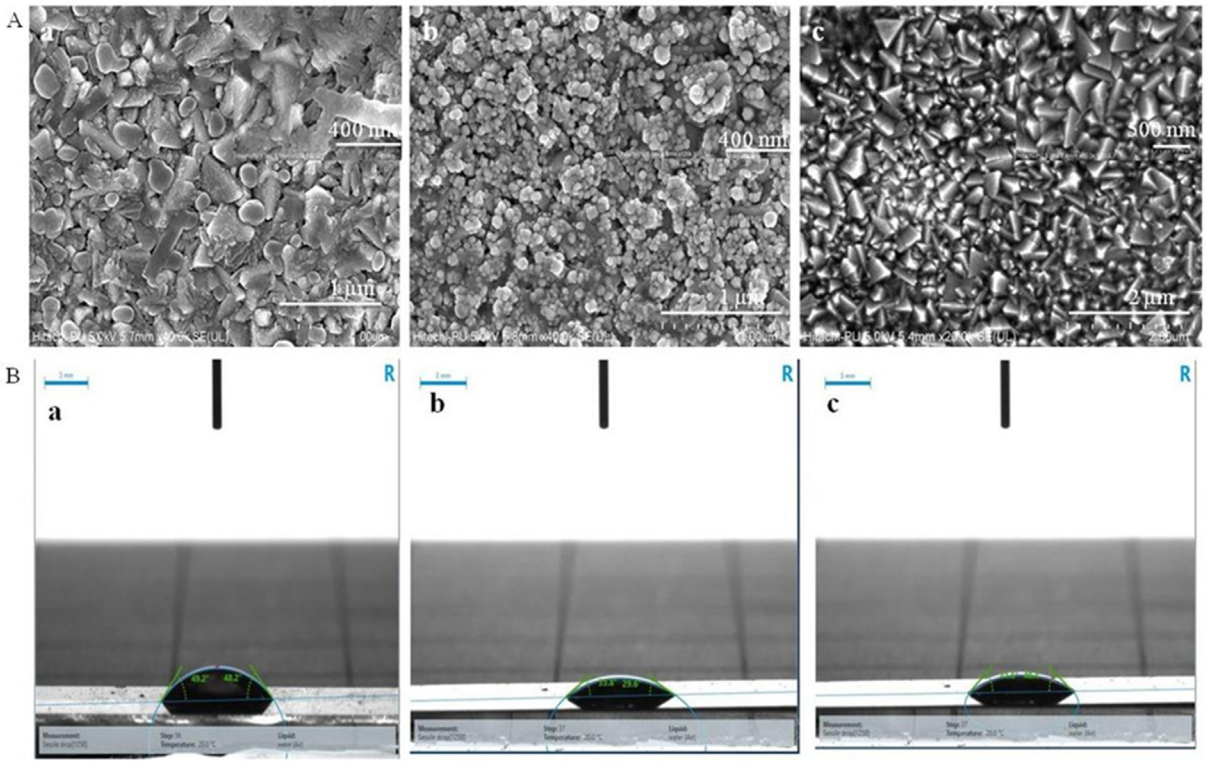

Fig. 3. (A) FE-SEM images of; and (B) Contact angle measurements using deionized water of (a) MoS_2NF-GNR/FTO, (b) MoS_2NF-GNR@AuNPs/FTO and (c) Spi/MoS_2NF-GNR@AuNPs/FTO.

1709 cm^{-1} are attributed to C—O stretch of the purine and pyrimidine rings of RNA respectively.

3.4. FE-SEM and contact angle measurements

The FE-SEM images of the electrode (Fig. 3A) exhibits the successful coating of the nanocomposites on the surface. As shown in Fig. 3A (a), the roughness on the electrode represents the deposition of MoS_2NF-GNR hybrid composite. Further, the electrodeposition of spherical AuNPs on the surface of the electrode provides larger surface area for immobilization of the biorecognition element (Fig. 3A (b)). The immobilization of spiegelmer molecules shows more rough surface as depicted in Fig. 3A (c), indicating successful attachment of biomolecule to the nanocomposite. All these results confirmed that the surface morphology of the electrode was modified at each step. The EDS mapping analysis was also done to characterize the composition of the fabricated materials (Fig. S1).

To further confirm the changes with each modification step, contact angle measurements were done (Fig. 3B). The deposition of hybrid nanocomposite on the electrode showed the contact angle of about 48.70° (Fig. 3B (a)). Next, the deposition of hydrophilic AuNPs lead to the decrease in the contact angle to 31.70° (Fig. 3B (b)). However, on spiegelmer immobilization, the contact angle was found to be increased to 41.0° due to the hydrophobic nature of oligonucleotides (Fig. 3B (c)). All the above observed results confirmed the proper fabrication of the biosensing platform.

3.5. Detection limit and range of the spiegelmer sensor

The optimal conditions for the best performance of the sensing platform were assessed. To obtain the optimal analytical performance, 10 μM spiegelmer concentration, 40 min of incubation time for target capturing and buffer of pH-7.0 were selected for performing all the electrochemical measurements. The detailed information has been provided in the Supplementary Information (Fig. S2).

The electrochemical measurements were carried out to assess the detectability of the sensing platform for different concentrations of hepcidin. Each measurement at different concentrations of hepcidin (n = 3) were examined using different electrode. The impedance signal increased with the increase in hepcidin concentration due to the formation of kinetic barrier for electron transfer with increasing hepcidin molecules binding to the immobilized spiegelmer on the electrode array. To evaluate the role of each nanomaterial used in the fabrication of FTO electrode, different set of electrodes i.e. FTO/Spi, FTO/GNR/Spi, FTO/MoS_2NF/Spi, FTO/MoS_2NF-GNR/Spi and FTO/AuNPs/Spi were prepared and the electrochemical measurements were performed. In FTO/Spi, a stationary relationship was observed between logarithm of hepcidin concentration and the impedance due to the non-binding of spiegelmer directly onto the electrode (Fig. 4A). In the case of FTO/GNR/Spi, FTO/MoS_2NF/Spi, FTO/MoS_2NF-GNR/Spi and FTO/AuNPs/Spi, a favorable linear relationship between logarithm of hepcidin concentration in the range 0.005–10 $ngmL^{-1}$ and the impedance was observed. Due to the conductive properties of graphene and gold, the FTO/GNR/Spi and FTO/AuNPs/Spi electrodes exhibited detection limits of 0.437 $pgmL^{-1}$ (regression coefficient $R^2 = 0.995$), and 0.379 $pgmL^{-1}$ ($R^2 = 0.999$) as calculated from the linear equations $y = 0.137x+1.168$ and $y = 0.158x+1.137$ respectively (Fig. 4B&E). The semi-conductive nature of molybdenum disulfide in FTO/MoS_2NF/Spi increases the detection limit to 0.588 $pgmL^{-1}$ ($R^2 = 0.996$) calculated from the linear equation $y = 0.102x+1.233$ (Fig. 4C). In FTO/MoS_2NF-GNR/Spi, the graphene in the MoS_2NF-GNR hybrid increases the electron flow which results in detection of hepcidin as low as 0.476 $pgmL^{-1}$ (R^2 = 0.998) from the

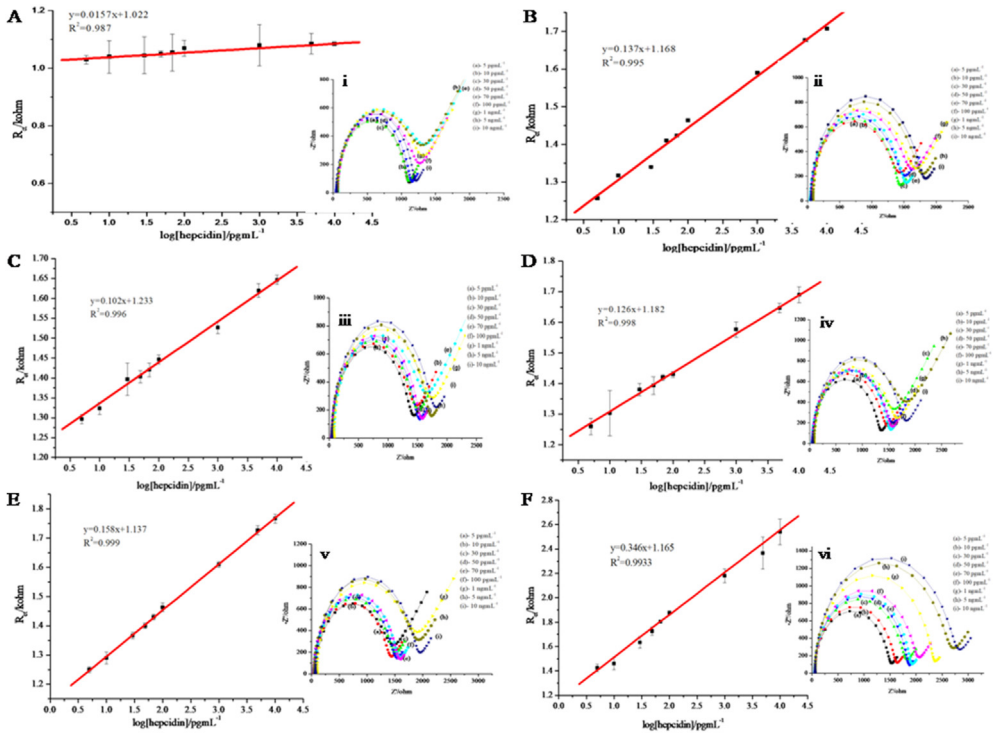

Fig. 4. (A–F) Calibration plot (range: 0.005–10 ngmL^{-1}) between ΔR_{ct} and logarithm of hepcidin concentration (n = 3) (Frequency: 10^{-1} to 10^{5} Hz and Potential: 0.18 V); (inset i-vi) Faradaic impedance spectra at different hepcidin concentrations (range: 5 pgmL^{-1}-10 ngmL^{-1}) of A) FTO/Spi, B) FTO/GNR/Spi, C) FTO/MoS_2NF/Spi, D) FTO/MoS_2NF-GNR/Spi, E) FTO/AuNPs/Spi and F) FTO/MoS_2NF-GNR@AuNPs/Spi.

Table 1
Comparison of biosensors for hepcidin detection with present work.

S.No	Method	Materials used	Sample matrix	Analyte	Range	LOD	Ref
1.	Optical	Molecular imprinted polymer nanoparticles/Biotin NeutrAvidin™	Human serum	Hepcidin	7.2–720 pM	13.5 pgmL^{-1}	[37]
2.	Optical	Anti-hep/streptavidin/carboxylated dextran CM5 biochip Or Biotin-HBD/streptavidin/carboxylated dextran CM5 biochip	Standard samples	Hepcidin	1–100 ngmL^{-1} or 0.3–3 mgL^{-1}	1.8 ± 0.6 ngmL^{-1} or 341 ± 0.6 mgL^{-1}	[5]
3.	Electrochemical	Anti-hep/Cys/Ag@Au NPs/FTO	Human serum	Hepcidin	0.01–100 ngmL^{-1}	0.857 pgmL^{-1}	[38]
4.	Electrochemical	Spi/MoS_2NF-GNR@AuNPs/FTO	Human serum	Hepcidin	0.01–100 ngmL^{-1}	0.173 pgmL^{-1}	Present work

y = 0.126x+1.182 equation (Fig. 4D). On the contrary, the proposed spiegelmer FTO/MoS_2NF-GNR@AuNPs/Spi sensor exhibited the detection limit of 0.173 pgmL^{-1} (R^2 = 0.993) from the linear equation as y = 0.346x+1.165 (Fig. 4F) which was much lower in comparison to the biosensors fabricated with individual nanomaterials due to the highly conductive nature of the nanocomposite (MoS_2NF-GNR@AuNPs). The LOD was determined using the following equation: 3 s/m, where s represented the standard deviation of the measured impedance signals for the blank and m represented the slope of the linear calibration curve [34].

The developed spiegelmer sensor clearly shows the significant dynamic range as well as LOD in comparison to other biosensors reported for hepcidin quantification (Table 1). The conventional competitive ELISA detects hepcidin as low as 21 μgL^{-1} [35] and HPLC/MS/MS has limit of quantification as 0.1 nmol L^{-1} [36]. Furthermore, the commercially available kits for hepcidin detection reports quantification in the following dynamic range: R&D Systems (15.6–1000 pgmL^{-1}), DRG Diagnostics (0.135–81 ngmL^{-1}), Cloud Clone Corp. (0.320–200 ngmL^{-1}) and Intrinsic Lifesciences (2.5–1000 ngmL^{-1}). As shown in Table 1, the proposed spiegelmer sensor exhibited excellent performance in terms of detection limit as well as wider dynamic range as compared to other biosensors. The L-configuration of the spiegelmer allowed the binding of hepcidin to it with greater affinity than D-RNA aptamers or antibodies, thus, resulting in lowest LOD towards hepcidin so far. Hence, this biosensor holds good potential for clinical applications.

3.6. Selectivity and stability assay

To study selectivity of the spiegelmer sensor towards hepcidin, various interfering agents were used such as BSA (1 μgmL^{-1}), glucose (1 μgmL^{-1}), cholesterol (5 μgmL^{-1}), somatostatin (SST; 100 nM) and MUC1 (100 nM). As seen in Fig. 5A, the low signal response was observed for the interfering agents due to non-specific interactions with the spiegelmer, whereas in case of mixture, the impedance response was significantly high confirming the selective binding of hepcidin with the spiegelmer. To further confirm the specificity, electrochemical measurements were

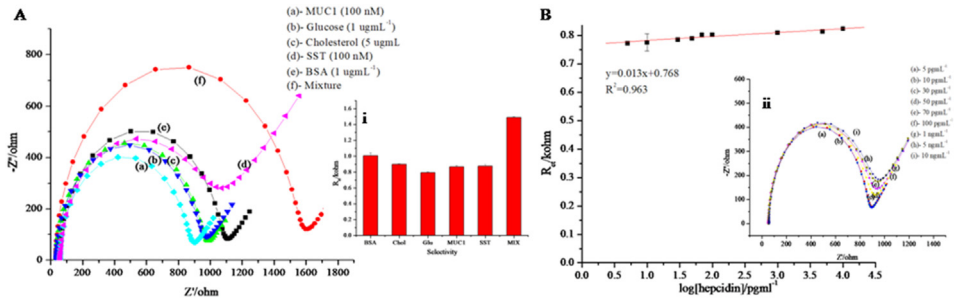

Fig. 5. (A) Selectivity of spiegelmer sensor towards hepcidin (n = 3); inset (i) represents the R_{ct} values of the different interference agents (n = 3); (B) Calibration plot between ΔR_{ct} and logarithm of hepcidin concentration (n = 3); inset (ii) Faradaic impedance spectra at different hepcidin concentrations (range: 5 $pgmL^{-1}$-10 $ngmL^{-1}$) of FTO/MoS_2NF-GNR@AuNPs.

Table 2
The recovery percentage of hepcidin in spiked-in serum samples.

Sample	Spiked ($pgmL^{-1}$)	Found by designed spiegelmer sensor ($pgmL^{-1}$)	Recovery (%, n = 3)	RSD (%)
1	5	4.82	96.4	3.22
2	10	9.79	97.9	1.88
3	50	46.5	93.0	0.95
4	100	103.1	103.1	1.02
5	1000	952.7	95.2	1.4
6	10000	8981.2	89.8	3.62

performed for two different sets of electrodes i.e. FTO/MoS_2NF-GNR@AuNPs and FTO/MoS_2NF-GNR@AuNPs/Spi. Both these electrodes were subjected to different concentrations of hepcidin ranging from 5 $pgmL^{-1}$ to 10 $ngmL^{-1}$ and the change in impedance was recorded. It was observed that in absence of spiegelmer onto the electrode, there was no significant change in the impedance signal with increasing concentration of hepcidin (Fig. 5B), whereas, in FTO/MoS_2NF-GNR@AuNPs/Spi, a linear relationship was recorded between logarithm of hepcidin concentration in the range 0.005–10 $ngmL^{-1}$ and the impedance (Fig. 4F). Thus, it could be inferred that spiegelmer is imperative for capturing of hepcidin molecules.

The stability of Spi/MoS_2NF-GNR@AuNPs biosensor was also investigated under optimal conditions for a period of 25 days. The spiegelmer sensor retained 88.6% of the original signal until 20 days and then sharply declined to 73.74% after 25 days (Fig. S3). The considerably good shelf-life of 20 days at 4 °C by retaining about 88.6% activity of its initial value was most likely due to the stability of the immobilized spiegelmer and retention of its biological activity on the electrode. The results suggested that the sensor possessed satisfactory shelf-life.

3.7. Regeneration, reproducibility and repeatability assay

To assess the reusability of the proposed spiegelmer sensor, regeneration experiment was conducted. The same electrode was regenerated using 10 mM NaOH and the impedance was recorded each time. For five cycles, the reduction in impedance response recorded was 92.8 %, 87.45 %, 84.04 %, 74.36 %, and 64.79 % as shown in Fig. S4. The decline in signal may be attributed to the disruption of Au-thiol linkage responsible for spiegelmer immobilization on the electrode surface.

The reproducibility assay was performed using fifteen independent electrodes, each incubated with 100 $pgmL^{-1}$ hepcidin for 40 min. The EIS response was measured and the RSD % of 5.46 % was observed indicating that the designed biosensor had good reproducibility. For repeatability, the same spiegelmer sensor was used repetitively for five times in a day at different times and the impedance signals were recorded. The RSD 4.76 % obtained was showing acceptable repeatability of the spiegelmer sensor.

3.8. Analysis of spiked-in serum sample

To further validate the analytical performance of the spiegelmer sensor, different concentrations of hepcidin spiked in 10 % human serum samples were determined as recovery percentages (Table 2). The recovery yield was in the range of 89.8–103.1 % for the spiked-in human serum sample. As shown in Fig. 6A and B, the impedance

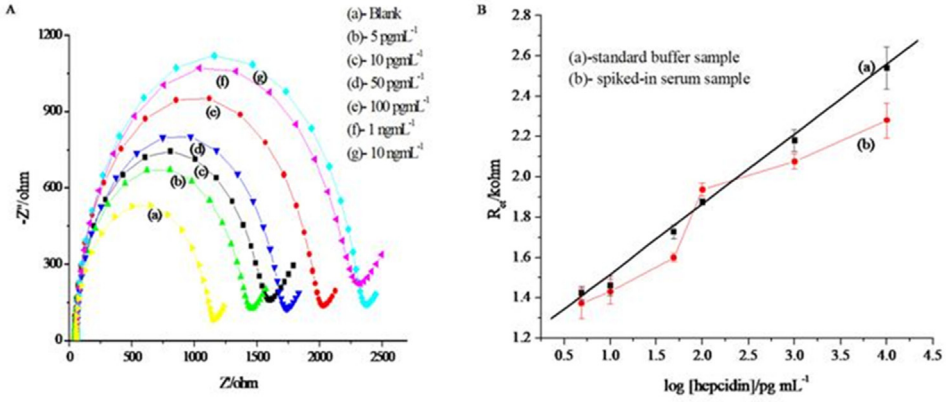

Fig. 6. (A) EIS recorded for varying concentration of hepcidin in spiked human serum (blank to 10 $ngmL^{-1}$). (B) The calibration curve between R_{ct} (kohm) vs. logarithm of concentration of hepcidin ($pgmL^{-1}$) in (i) buffer solution and (ii) spiked serum sample.

spectra and the R_{ct} value respectively, increased with increasing spiked-in hepcidin concentration indicating that the proposed spiegelmer sensor had good accuracy for the determination of hepcidin in human serum sample.

4. Conclusions

This study presented a novel impedimetric spiegelmer sensor based on MoS_2NF-GNR@AuNPs for the detection of hepcidin. The thiolated spiegelmer anchored onto MoS_2NF-GNR@AuNPs provided high affinity towards the hepcidin which helped in achieving lower detection limit (0.173 $pgmL^{-1}$) within a wide linear range (0.005–10 $ngmL^{-1}$). The selectivity study revealed that the sensor had successful anti-interference property and considerably good shelf life of 20 days. The practical application of proposed sensor assessed in spiked-in serum samples suggested that the developed sensing platform offered a reliable diagnostic strategy for the determination of hepcidin in clinical samples.

CRediT authorship contribution statement

Shilpa Rana: Conceptualization, Methodology, Formal analysis, Investigation, Writing – original draft, Writing – review & editing. **Amandeep Kaur:** Visualization. **Anu Bharti:** Visualization. **Suman Singh:** Resources, Supervision. **Archana Bhatnagar:** Supervision. **Nirmal Prabhakar:** Project administration, Writing – review & editing, Supervision.

Declaration of competing interest

The authors declare that they have no known competing financial interests or personal relationships that could have appeared to influence the work reported in this paper.

Acknowledgements

The research was financial supported by DST-SERB [EEQ/2017/000239], DST-Purse II and Special Assistance Programme (UGC-SAP) [F.4-7/2015/DRS-III (SAP-II)]. The authors acknowledge the Central instrument laboratory, Panjab University for instrumentation facilities. I would also like to thank and acknowledge UGC-NET for providing the award of fellowship [19/06/2016(i)-EU-V].

Appendix A. Supplementary data

Supplementary data to this article can be found online at https://doi.org/10.1016/j.aca.2021.338863.

References

[1] D.J. Hare, Hepcidin: a real-time biomarker of iron need, Metall 9 (2017) 606–618.
[2] I.M. Abbas, H. Hoffmann, M. Montes-Bayón, M.G. Weller, Improved LC-MS/MS method for the quantification of hepcidin-25 in clinical samples, Anal. Bioanal. Chem. 410 (2018) 3835–3846.
[3] K.C. Cho, B.K. Cho, J.W. Jung, Y.J. Lee, E.B. Lee, E.C. Yi, SRM-MS method development for hepcidin-25 peptide, Journal of analytical methods in chemistry, 2018 (2018) 9653747.
[4] P. Gutschow, H. Han, G. Olbina, K. Westerman, E. Nemeth, T. Ganz, K. Copeland, M. Westerman, V. Ostland, Clinical immunoassay for human hepcidin predicts iron deficiency in first-time blood donors, The journal of applied laboratory medicine 5 (2020) 943–953.
[5] S. Scarano, A. Vestri, M.L. Ermini, M. Minunni, SPR detection of human hepcidin-25: a critical approach by immuno- and biomimetic-based biosensing, Biosens. Bioelectron. 40 (2013) 135–140.
[6] L. Cenci, E. Andreetto, A. Vestri, M. Bovi, M. Barozzi, E. Iacob, M. Busato, A. Castagna, D. Girelli, A.M. Bossi, Surface plasmon resonance based on molecularly imprinted nanoparticles for the picomolar detection of the iron regulating hormone Hepcidin-25, J. Nanobiotechnol. 51 (2015) 51.
[7] S. Ni, Z. Zhuo, Y. Pan, Y. Yu, F. Li, J. Liu, L. Wang, X. Wu, D. Li, Y. Wan, L. Zhang, Z. Yang, B.-T. Zhang, A. Lu, G. Zhang, Recent progress in aptamer discoveries and modifications for therapeutic applications, ACS Appl. Mater. Interfaces 13 (2020) 9500–9519.
[8] F. Schwoebel, L.T. van Eijk, D. Zboralski, S. Sell, K. Buchner, C. Maasch, W.G. Purschke, M. Humphrey, S. Zöllner, D. Eulberg, F. Morich, P. Pickkers, S. Klussmann, The effects of the anti-hepcidin Spiegelmer NOX-H94 on inflammation-induced anemia in cynomolgus monkeys, Blood 121 (2013) 2311–2315.
[9] A. Vater, S. Klussmann, Turning mirror-image oligonucleotides into drugs: the evolution of Spiegelmer® therapeutics, Drug Discov. Today 20 (2015) 147–155.
[10] S. Klussmann, A. Nolte, R. Bald, V.A. Erdmann, J.P. Fürste, Mirror-image RNA that binds D-adenosine, Nat. Biotechnol. 14 (1996) 1112–1115.
[11] Z. Li, L. Wang, Y. Li, Y. Feng, W. Feng, Carbon-based functional nanomaterials: preparation, properties and applications, Compos. Sci. Technol. 179 (2019) 10–40.
[12] K.P. Delgado, P.A. Raymundo-Pereira, A.M. Campos, O.N. Oliveira Jr., B.C. Janegitz, Ultralow cost electrochemical sensor made of potato starch and carbon black nanoballs to detect tetracycline in waters and milk, Electroanalysis 30 (2018) 2153–2159.
[13] P.A. Raymundo-Pereira, N.O. Gomes, F.M. Shimizu, S.A.S. Machado, O.N. Oliveira, Selective and sensitive multiplexed detection of pesticides in food samples using wearable, flexible glove-embedded non-enzymatic sensors, Chem. Eng. J. 408 (2021) 127279.
[14] A.M. Campos, P.A. Raymundo-Pereira, C.D. Mendonça, M.L. Calegaro, S.A.S. Machado, O.N. Oliveira, Size control of carbon spherical shells for sensitive detection of paracetamol in sweat, saliva, and urine, ACS Applied Nano Materials 1 (2018) 654–661.
[15] L. Jothi, S.K. Jaganathan, G. Nageswaran, An electrodeposited Au nanoparticle/porous graphene nanoribbon composite for electrochemical detection of alpha-fetoprotein, Mater. Chem. Phys. 242 (2019) 122514.
[16] J. Bai, Y. Huang, Fabrication and electrical properties of graphene nanoribbons, Mater. Sci. Eng. R Rep. 70 (2010) 341–353.
[17] K.-J. Huang, Y.-J. Liu, Y.-M. Liu, L.-L. Wang, Molybdenum disulfide nanoflower-chitosan-Au nanoparticles composites based electrochemical sensing platform for bisphenol A determination, J. Hazard Mater. 276 (2014) 207–215.
[18] H. Gu, L. Zhang, Y. Huang, Y. Zhang, W. Fan, T. Liu, Quasi-one-dimensional graphene nanoribbon-supported MoS2 nanosheets for enhanced hydrogen evolution reaction, RSC Adv. 6 (2016) 13757–13765.
[19] M. Asad, S. Salimian, M.H. Sheikhi, M. Pourfath, Flexible phototransistors based on graphene nanoribbon decorated with MoS2 nanoparticles, Sensor Actuator Phys. 232 (2015) 285–291.
[20] Y. Liu, X. Wang, X. Song, Y. Dong, L. Yang, L. Wang, D. Jia, Z. Zhao, J. Qiu, Interlayer expanded MoS2 enabled by edge effect of graphene nanoribbons for high performance lithium and sodium ion batteries, Carbon 109 (2016) 461–471.
[21] P. Zhao, M. Ni, Y. Xu, C. Wang, C. Chen, X. Zhang, C.-Y. Li, Y. Xie, J. Fei, A novel ultrasensitive electrochemical quercetin sensor based on MoS2 - carbon nanotube @ graphene oxide nanoribbons/HS- cyclodextrin/graphene quantum dots composite film, Sensor. Actuator. B Chem. 299 (2019) 126997.
[22] M.H.M. Facure, R. Schneider, D.M. dos Santos, D.S. Correa, Impedimetric electronic tongue based on molybdenum disulfide and graphene oxide for monitoring antibiotics in liquid media, Talanta 217 (2020) 121039.
[23] R. Bar-Ziv, P. Ranjan, A. Lavie, A. Jain, S. Garai, A. Bar Hen, R. Popovitz-Biro, R. Tenne, R. Arenal, A. Ramasubramaniam, L. Lajaunie, M. Bar-Sadan, Au-MoS2 hybrids as hydrogen evolution electrocatalysts, ACS Appl. Energy Mater. 2 (2019) 6043–6050.
[24] J. Zhou, Y.N. Zhao, J. Bao, D. Huo, H. Fa, X. Shen, C. Hou, One-step electrodeposition of Au-Pt bimetallic nanoparticles on MoS 2 nanoflowers for hydrogen peroxide enzyme-free electrochemical sensor, Electrochim. Acta 250 (2017) 152–158.
[25] S. Su, Z. Lu, J. Li, Q. Hao, W. Liu, C. Zhu, X. Shen, J. Shi, L. Wang, MoS2–Au@Pt nanohybrids as a sensing platform for electrochemical nonenzymatic glucose detection, New J. Chem. 42 (2018) 6750–6755.
[26] Z. Gao, Y. Li, X. Zhang, J. Feng, L. Kong, P. Wang, Z. Chen, Y. Dong, Q. Wei, Ultrasensitive electrochemical immunosensor for quantitative detection of HBeAg using Au@Pd/MoS2@MWCNTs nanocomposite as enzyme-mimetic labels, Biosens. Bioelectron. 102 (2018) 189–195.
[27] Q. Liu, J. Huan, A. Fei, H. Mao, K. Wang, "Signal on" electrochemiluminescence pentachlorophenol sensor based on luminol-MWCNTs@graphene oxide nanoribbons system, Talanta 134 (2015) 448–452.
[28] F. Ran, H. Liu, X. Wang, Y. Guo, A novel molybdenum disulfide nanosheet self-assembled flower-like monolithic sorbent for solid-phase extraction with high efficiency and long service life, J. Chromatogr., A 1507 (2017) 18–24.
[29] P. Georgiev, S. Simeonova, A. Chanachev, L. Mihaylov, D. Nihtianova, K. Balashev, Acceleration effect of copper(II) ions on the rate of citrate synthesis of gold nanoparticles, Colloid. Surface. Physicochem. Eng. Aspect. 494 (2016) 39–48.
[30] C. Vericat, M.E. Vela, G. Corthey, E. Pensa, E. Cortés, M.H. Fonticelli, F. Ibañez, G.E. Benitez, P. Carro, R.C. Salvarezza, Self-assembled monolayers of thiolates on metals: a review article on sulfur-metal chemistry and surface structures, RSC Adv. 4 (2014) 27730–27754.
[31] R. Elshafey, A.C. Tavares, M. Siaj, M. Zourob, Electrochemical impedance immunosensor based on gold nanoparticles–protein G for the detection of

cancer marker epidermal growth factor receptor in human plasma and brain tissue, Biosens. Bioelectron. 50 (2013) 143–149.
[32] H. Nautiyal, S. Kumari, O.P. Khatri, R. Tyagi, Copper matrix composites reinforced by rGO-MoS2 hybrid: strengthening effect to enhancement of tribological properties, Compos. B Eng. 173 (2019) 106931.
[33] E. Akbarzadeh, F. Bahrami, M.R. Gholami, Au and Pt nanoparticles supported on Ni promoted MoS2 as efficient catalysts for p-nitrophenol reduction, Journal of Water Process Engineering 34 (2020) 101142.
[34] C. Ramírez, M.A. del Valle, M. Isaacs, F. Armijo, Electrochemical oxidation of catecholamines on fluorine-doped SnO2 substrates. Square-wave voltammetric method for methyldopa determination in pharmaceutical dosage forms, Electrochim. Acta 199 (2016) 227–233.
[35] T. Karlsson, Evaluation of a competitive hepcidin ELISA assay in the differential diagnosis of iron deficiency anaemia with concurrent inflammation and anaemia of inflammation in elderly patients, J. Inflamm. 14 (2017), 21-21.
[36] M. Chen, J. Liu, B. Wright, A sensitive and cost-effective high-performance liquid chromatography/tandem mass spectrometry (multiple reaction monitoring) method for the clinical measurement of serum hepcidin, Rapid Commun. Mass Spectrom. 34 (2020) e8644.
[37] L. Cenci, E. Andreetto, A. Vestri, M. Bovi, M. Barozzi, E. Iacob, M. Busato, A. Castagna, D. Girelli, A.M. Bossi, Surface plasmon resonance based on molecularly imprinted nanoparticles for the picomolar detection of the iron regulating hormone Hepcidin-25, J. Nanobiotechnol. 13 (2015), 51-51.
[38] S. Rana, A. Bharti, S. Singh, A. Bhatnagar, N. Prabhakar, Gold-silver core-shell nanoparticle–based impedimetric immunosensor for detection of iron homeostasis biomarker hepcidin, Microchimica Acta 187 (2020) 626.